











Tris(8-hydroxyquinoline)aluminium in a polymer matrix as an active layer for green OLED applications

Małgorzata Sypniewska¹, Monika Pokladko-Kowar², Anna Kaczmarek-Kedziera³, Iulia E. Brumboiu¹,
Viviana Figà⁴, Aleksandra Apostoluk⁵, Peng Song^{6,7}, Junyan Liu^{6,8}, Robert Szczesny³,
Ewa Gondek², Beata Derkowska-Zielinska^{1*}

¹Institute of Physics, Faculty of Physics, Astronomy and Informatics, Nicolaus Copernicus University in Torun, Grudziądzka 5, Torun 87-100, Poland

²Department of Physics, Cracow University of Technology, Podchorążych 1, 30-084 Krakow, Poland

³Faculty of Chemistry, Nicolaus Copernicus University in Torun, Gagarina 7, Torun 87-100, Poland

⁴Dipartimento di Scienze e Tecnologie Biologiche, Chimiche e Farmaceutiche, Università di Palermo, Viale delle Scienze, Parco d'Orleans II, 90128 Palermo, Italy

⁵Université de Lyon, INSA Lyon, ECL, CNRS, UCBL, CPE Lyon, INL, UMR5270, 69621 Villeurbanne, France

⁶State Key Laboratory of Robotics and System, Harbin Institute of Technology, Harbin, 150001, China

⁷School of Instrumentation Science and Engineering, Harbin Institute of Technology, Harbin, 150001, China

⁸School of Mechatronics Engineering, Harbin Institute of Technology, Harbin, 150001, China

Article info

Article history:

Received 28 Feb. 2023

Received in revised form 06 May 2023

Accepted 21 May 2023

Available on-line 12 Jun. 2023

Keywords:

Tris(8-hydroxyquinoline)aluminium;
OLED;
photo- and electro-luminescence;
spectroscopic ellipsometry;
DFT calculation.

Abstract

Tris(8-hydroxyquinoline)aluminium with poly(N-vinylcarbazole) (Alq₃:PVK) or polystyrene sulfonate (Alq₃:PSS) were deposited by spin-coating on glass and silicon substrates. SEM measurements show that relatively smooth thin films were obtained. Fourier transform infrared measurements were performed to confirm the composition of the samples. The optical properties of thin films containing Alq₃:PVK and Alq₃:PSS were characterised using absorption spectroscopy and spectroscopic ellipsometry. It was found that the absorption spectrum of Alq₃:PVK is characterised by four bands, while for Alq₃:PSS only three bands are visible. The photoluminescence of the studied thin layers shows a peak with a maximum at about 500 nm. Additionally, cyclic voltammetry of Alq₃ is also presented. Theoretical density functional theory calculations provide the insight into the interaction and nature of Alq₃:PVK and Alq₃:PSS excited states. Finally, the organic light-emitting diode (OLED) structure based on Alq₃:PVK was fabricated and showed strong electro-luminescence with a green emission at 520 nm. The results of the device show that the ITO/PEDOT:PSS/Alq₃:PVK/Ca/Al system can be useful for the production of low-cost OLEDs with Alq₃:PVK as an active layer for future lighting applications.

1. Introduction

There is a growing interest in organic light-emitting diodes (OLEDs) thanks to their high brightness, high efficiency, low-cost and easy production of large area devices [1, 2], and availability of a wide range of emission colours [3]. The ability to transfer charge to the electrode and effectively transport charge, as well as fluorescence, are fundamental requirements for organic electroluminescent materials (ELMs). Various organic materials (OMs) were tested as an active component of a device to optimize

its efficiency [4]. Due to the molecular structure of OMs, they can be divided into one of four groups as follows: conjugated polymers, conjugated oligomers, backbone polymers with isolated chromophores and side chain polymers with linked chromophores, which include low molecular weight materials (such as metal chelates). Conjugated polymers are in other words organic semiconductors with delocalized π -molecular orbitals along the polymeric chain. Various types of conjugated polymers have been developed, for example: polyacetylene, polyaniline, polythiophene, poly(p-phenylene), poly(p-phenylene vinylene), polypyrrole, etc. [5]. Conjugated oligomers, thanks to strict control of the effective conjugation length

*Corresponding author at: beata@fizyka.umk.pl

and precisely defined structure, have been used as new materials in electro-optical applications [5].

Poly(p-phenylene vinylene) (PPV) was the first conjugated polymer used to make OLEDs [6]. In the ITO/PPV/Al device configuration, emission in the yellow-green part of the electromagnetic spectrum and significant charge injection just below 14 V was observed, and an external quantum efficiency of 0.05% was achieved. Poly(3,4-ethylenedioxythiophene):poly(styrene sulfonate) (PEDOT:PSS), as a conductive polymer, is widely used in optoelectronic applications due to its high conductivity, as well as excellent mechanical properties. PEDOT:PSS is considered one of the most famous and important electronic materials due to its high electronic conductivity, which at room temperature exceeds 1000 S/cm [7, 8]. This makes it a potential candidate for use as a transparent conductive material to replace indium tin oxide (ITO) and reduce the cost of producing flexible films [8]. In chemical structure, PEDOT and PSS molecules are built as a sequence of monomers. The secondary structure of PEDOT and PSS is a polyionic complex where they are connected by electrostatic interactions, and PSS acts as a counter-ion to balance the charge transfer, resulting in PEDOT hole carriers [9]. The disadvantages of PEDOT:PSS include: insufficient conductivity, sensitivity to air, poor adhesion to hydrophobic substrates [10], or poor lifetime which limits its use in OLEDs [11, 12].

Tris(8-hydroxyquinoline)aluminium (Alq_3) can be used in the development of long-life OLEDs [13], as well as organic solid-state lasers, large-screen displays, and organic solar cells [14]. In 1987, Tang and Van Slyke reported the first high-performance OLED display, which was built with two active layers with Alq_3 serving as an electron transporting material and an emitting layer [15]. The basic requirement in the broadcast technology is to guarantee the appropriate stability of the device. Many studies have been conducted and it has been found that the efficiency of OLEDs is influenced by the manufacturing processes. For example, the efficiency of OLEDs with Alq_3 depends on the material deposition rate [16, 17]. Despite the high luminescence efficiency [18], Alq_3 -based OLEDs show poor luminescence stability. In OLEDs based on Alq_3 , the time needed to lower the luminance to half of its initial value (diode half-life) is only a few hundred hours [19]. Therefore, research into the use of Alq_3 in OLEDs is important and still needed.

In OLEDs, Alq_3 is used as the green emitter and electron transport layer. Perez-Bolivar *et al.* investigated whether its normal blue-green luminescence could be fine-tuned by adding substitution groups into the Alq_3 structure [20]. They found that the presence of methyl substituents in Alq_3 causes a hypsochromic luminescence shift, which can be attributed to the shift in the energy of the lowest unoccupied molecular orbital (LUMO) level. In contrast, modification of the Alq_3 structure with F or CN groups can lower the energy of highest occupied molecular orbital (HOMO) levels, causing blue emission with a wavelength of 480 nm. Multilayer devices containing Alq_3 (i.e., PEDOT:PSS/NPD/ Alq_3 /CsF/Al) showed a high luminance of 52300 cd/m² for a turn-on voltage of 5.5 V [20]. Zhang, *et al.* produced a diode like ITO/PEDOT/PVK: Alq_3 /Ca/Al [21]. They found that the electroluminescence (EL) efficiency of the produced OLED structure depends on the

concentration of Alq_3 and poly(9-vinylcarbazole) (PVK). In addition, it was found that the device with Alq_3 :PVK film, where the ratio of Alq_3 :PVK is 2:10, showed the maximum efficiency of EL. This indicates that the electron and hole transport balance in such a layer can be reached by adjusting the concentration of Alq_3 in PVK. A decrease in EL efficiency in extreme cases (i.e., low and high concentrations of Alq_3 in PVK) can be observed, which can be attributed to unbalanced transport of electron and hole. They also found that in the PVK: Alq_3 layer, the hole mobility decreased when the Alq_3 content increased, which was interpreted as increasing the hole hopping distance during Alq_3 mixing. Thus, the charge carriers mobility can be adjusted by changing the composition of the Alq_3 :PVK mixture to achieve a balance of electron and hole transport and improve the performance of OLED display. Fukushima *et al.* fabricated OLED with a structure of ITO/a-NPD/ Alq_3 /Cs₂CO₃/Al, using three kinds of crystalline polymorphs of Alq_3 powder (i.e., α - Alq_3 , δ - Alq_3 , or $\alpha\gamma\delta$ - Alq_3) [22]. All these OLEDs showed green EL at about 525 nm, independent of the crystalline Alq_3 polymorph before vacuum deposition. They also showed that the EL efficiency of OLEDs made of δ - Alq_3 and $\alpha\gamma\delta$ - Alq_3 (mixture of α -, γ -, and δ -forms) was increased by a factor of 1.1 and 1.4, respectively, compared to the case of α - Alq_3 for the same device structure.

In this work, we focus on the study of differences in the properties of Alq_3 dispersed in PVK and polystyrene sulfonate (PSS) polymer matrices. This issue is very important due to the efficiency of the produced OLEDs. Thus, Alq_3 powder was dispersed in PVK or PSS polymer matrices, and then Alq_3 :polymer (i.e., Alq_3 :PVK or Alq_3 :PSS) was deposited on glass or silicon substrates by spin-coating technique. The optical and structural properties of thin layers obtained in this way were investigated using ultraviolet-visible (UV-VIS), spectroscopic ellipsometry (SE) and infrared (IR) spectroscopies, as well as scanning electron microscopy (SEM). The photo-luminescence (PL) of the Alq_3 :polymer thin layers was also analysed. Finally, a simple OLED structure (i.e., ITO/PEDOT:PSS/ Alq_3 :PVK/Ca/Al) was prepared, and its EL was measured. To the best of our knowledge, the ITO/PEDOT:PSS/ Alq_3 :PVK/Ca/Al structure with Alq_3 :PVK as the active film is described here for the first time. Additionally, experimental results of cyclic voltammetry of Alq_3 and theoretical density functional theory (DFT) calculations of Alq_3 :polymer model systems are also presented, which were aimed at estimating the energy of HOMO-LUMO levels of the studied layers, as well as the theoretical estimation of OLED parameters.

2. Materials and methods

2.1. Materials

Tris(8-hydroxyquinoline)aluminium, poly N-vinylcarbazole ($M_w \sim 1000000$ g/mol) and poly(styrene sulfonate) ($M_w \sim 70000$ g/mol) powders were bought from Sigma-Aldrich.

Alq_3 is a chelate formed by an aluminium metal ion (Al^{3+}) and three molecules of 8-hydroxyquinoline which can arrange to form a facial [see Fig. 1(a)] or meridional Alq_3 isomer [22]. The HOMO (π orbitals) states are found

on the phenoxide (O) ring of quinoline, while the LUMO (π^* orbitals) is located mainly on the pyridyl (N) side [23]. Alq₃ has strong stability in a dry environment because the electronic structure of Al³⁺ (1s²2s²2p⁶) is similar to the atomic structure of the corresponding inert gas [24]. Alq₃ is thermally stable. Its glass transition temperature is 172 °C. Due to the intrinsic behaviour of Alq₃ in the polymorphic phase, it can be easily thermally deposited to form amorphous layers [25].

Emission of PVK, the holes transport material, includes the whole blue region thanks to the carbazole groups [26]. PVK is widely used in the production of blue OLEDs [27], instead of conjugated polymers, which have low blue emission. PVK is an amorphous conductive polymer consisting of linear chains of repeating (H₂C–HC)_n groups with carbazole side groups ((C₆H₄)₂NH) randomly distributed around the same chain [see Fig. 1(b)]. These groups work as both electroluminescent chromophores and hole conducting centres, and are, therefore, mainly responsible for the electrical and electroluminescent properties of the polymer. The electrical conductivity in PVK is regulated by both field-assisted and temperature-activated hopping processes. PL, on the other hand, occurs through the radiation decay of Frenkel excitons. Charge transport in PVK is influenced by the presence of impurities, which can significantly reduce the mass conductivity and charge carrier injection [28].

PSS is built of a non-conjugated linear backbone with randomly oriented pendant functionalities [see Fig. 1(c)]. PSS has electrical insulating properties. PSS acts as a counterion to stabilize charge carriers, so it is essential for conductivity [29]. However, it is known that a large amount of hygroscopic PSS has a negative effect on the conductivity of the polymer electrode. In addition, PSS degrades the efficiency of OLEDs over time by acid attack on ITO anodes [30]. PSS is also hydrophilic, which makes OLEDs vulnerable to water in the air [31].

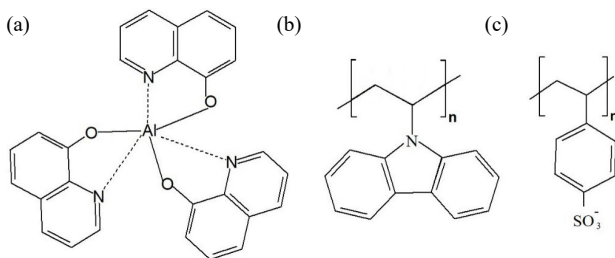


Fig. 1. Molecular structures of the facial Alq₃ isomer (a), PVK (b) and PSS (c).

2.2. Thin films preparation

PVK and PSS were dissolved in dichloroethane (HPLC ≥ 99.8%, Sigma Aldrich) for 24 h forming a 5% solution. To obtain Alq₃ solution with polymer, 0.02 g of Alq₃ powder was added to the ready solutions of polymer and put in an ultrasonic bath for about 30 min. The mixture of Alq₃:polymers was deposited on glass and silicon (p-Si (100)) substrates. Alq₃:polymer thin films were obtained using the spin-coating method (Spin-coater Laurell WS-650SZ-6NPP/A1/AR1/OND, 1600 rpm). Finally, the obtained films were dried for 24 h at room temperature.

2.3. OLED preparation

Figure 2(a) shows a fabricated multilayer device with the glass/ITO/PEDOT:PSS/Alq₃:PVK/Ca/Al structure.

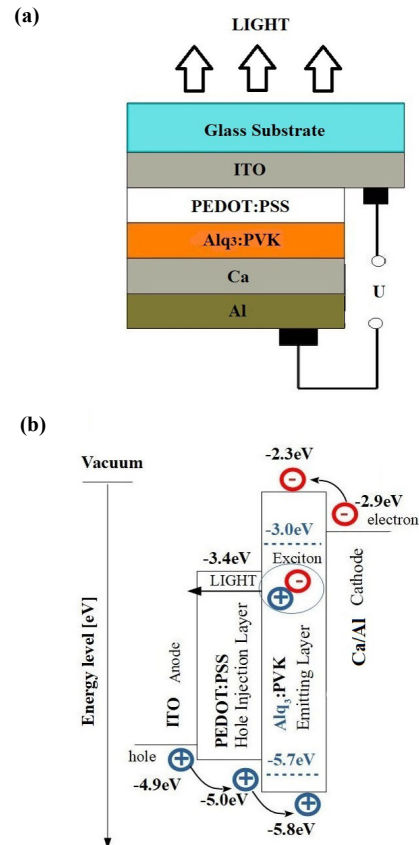


Fig. 2. OLED structure (a) and energy levels (b) of ITO/PEDOT:PSS/Alq₃:PVK/Ca/Al.

As illustrated in Fig. 2, the glass substrate was covered with an ITO layer (Sigma Aldrich, thickness of 118 nm, sheet resistance of 15 W/sq), which is an optically transparent anode in the system. The glass/ITO structure was then cleaned in an ultrasonic bath with isopropanol (P 99.5%), acetone (ACS reagent, P 99.5%), organic solvent (tetrahydrofuran (THF), anhydrous, 99.9%), detergent and distilled water [32]. Next, an aqueous solution of PEDOT:PSS (1.1 wt% dispersed in H₂O), which is a *p*-type organic semiconductor and hole transporting material, was deposited on the ITO. The thickness of the PEDOT:PSS spin-coated layer was 60 nm. The entire structure with PEDOT:PSS (surfactant free, high-conductive grade) was dried under vacuum (100 °C, 30 min.). The active layer represents 1.5% of Alq₃ in PVK. It turned out that this proportion provides the strongest electroluminescent emission. The mixture of Alq₃ and PVK was dissolved in THF (anhydrous, 99.9%) and the resulting solution was deposited on the PEDOT:PSS film under argon using a spin-coating technique. The Alq₃:PVK layer was about 103 nm thick. The obtained structure was dried (70 °C, 30 min.) to eliminate traces of THF. Finally, layers of calcium (Ca, 10 nm) and aluminium (Al, 100 nm) were evaporated on the Alq₃:PVK film under high vacuum (10⁻⁶ bar). An OLED structure was obtained with an active area of about 24 mm² [33]. All the powders and solvents used were purchased from Sigma-Aldrich.

Figure 2(b) shows the diagram of energy bands of individual layers in the ITO/PEDOT:PSS/Alq₃:PVK/Ca/Al system. The glass substrate supports the OLED. The highly transparent ITO layer is used as an anode for light visibility. ITO is also a good conductor with a high work function to facilitate the injection of holes into PEDOT:PSS. When a voltage is applied to the OLED electrodes, holes are injected and transported from ITO (anode) to Alq₃:PVK, i.e., the emitting layer (EML), via PEDOT:PSS, while electrons are injected and transported from Ca/Al (cathode) to EML. PEDOT:PSS is used as a hole injection layer (HIL) and facilitates hole injection from ITO to Alq₃:PVK. Thus, electron and hole carriers are transported to Alq₃:PVK, where recombination of electron-hole pairs occurs. It should be noted that PVK is responsible for transporting holes in this layer. The excitons produced in EML are returned to a ground state and emit light.

2.4. Experimental measurement methods and equipment

Fourier transform infrared (FTIR) spectra of Alq₃:polymer (i.e., Alq₃:PVK or Alq₃:PSS) deposited on Si substrates were obtained with FT-IR Vertex 70 V with a Hyperion 1000/2000 microscope by Bruker Optik from 200 to 2000 cm⁻¹. UV-VIS measurements of Alq₃:polymer thin films deposited on glass substrates were performed at room temperature using a Specord 200 spectrometer in the range of 270–600 nm. The photoluminescent signal of Alq₃:polymer layers deposited on Si substrates was detected using HITACHI f-2500 fluorescence spectrophotometer in the range of 420–600 nm ($\lambda_{\text{ex}} = 325$ nm, Xe lamp). SEM images of Alq₃:polymer films were recorded with a Quanta 3D FEG (FEI, Hillsboro, OR, USA) (EHT = 30 kV). Extinction coefficients and refractive indices of Alq₃:PVK active layer over the PEDOT:PSS/ITO/glass substrate were measured using Woollam M2000 spectroscopic ellipsometer (J. A. Woollam Co. Inc.) and analysed using CompleteEASE software. The Δ and Ψ ellipsometric angles were measured for three angles of incidence of light (i.e., 60°, 65°, and 70°) in the spectral range of 300–1200 nm. They are determined as the ratio of the amplitude reflection coefficients for *p*- and *s*-polarizations in the following way: $\rho = \frac{R_p}{R_s} = \tan \Psi e^{i\Delta}$, where Ψ – amplitude ratio and Δ – phase difference between *p*- and *s*-polarized light waves. The Tauc-Lorentz model with Gaussian oscillators was used to fit to the experimental data and to determine the layer parameters [34]. The Gaussian oscillators are described as follows:

$$\varepsilon_{2,N} = A_N e^{-\left(\frac{E-E_N}{B_r \sigma_N}\right)^2} - A_N e^{-\left(\frac{E+E_N}{B_r \sigma_N}\right)^2}, \quad (1)$$

where the fitting parameters often used to model thin polymer films are: A_N – absorption amplitude, B_r – boarding, and E_N – the oscillator energy, N – oscillators ($N = 6$, fitting for four Gaussian oscillators), and $\sigma_N = \frac{1}{2\sqrt{\ln 2}}$.

The EL of the OLED structure was detected at forward-bias voltages (ITO, positive; Ca/Al, negative) from 9 V to 15 V. The emitted light was recorded using a CCD spectrophotometer MS125 (Oriel Instruments Corp.) in the

range of 400–750 nm. The obtained device was exposed to air without encapsulation.

Alq₃ thin films were also characterised by electrochemical methods. These films were prepared by dissolving 1 mg of compound in 1 mL of THF. The solution was casted on the top of a flat glassy carbon electrode (diameter = 3 mm) and dried over night at room temperature. The glassy carbon was previously treated with a polishing pad using alumina suspension and rinsed in distilled water.

The electrochemical measurements were carried out in a three-electrode cell, using Ag/AgCl (3.0M KCl) as reference electrode, a graphite wire as counter electrode and modified glassy carbon as working electrode. Acetonitrile (CH₃CN, anhydrous 99.8%) containing 0.1M tetrabutylammonium hexafluorophosphate (TBAPF₆, electrochemical analysis 99%) was used as the electrolytic solution due to its electrochemical stability in a wide potential range. Cyclic voltammograms were recorded at room temperature, setting a potential scan rate of 100 mV/s and starting from the open circuit potential to +2.0V/(Ag/AgCl) via Ivium Vertex Potentiostat/Galvanostat.

All measurements were performed at room temperature.

2.5. Quantum-chemical calculations

The full optimization of the geometry for the facial (fac-Alq₃) and meridional (mer-Alq₃) isomers of Alq₃, polymer models and Alq₃:polymer complexes were performed within the ω B97X-D/def2-SVP approach in the gas phase. The nature of the stationary points on the potential energy surface was confirmed using harmonic vibrational analysis. The chain length of the polymer applied in the present study was limited to five mers, in order to provide enough flexibility and size to feature the interaction with the Alq₃ molecule and, at the same time, keep the calculation costs at a reasonable level. The HOMO-LUMO gap was confirmed to stabilize already for this size of the model. Three initial Alq₃:polymer arrangements, generated in a random way, were considered. The super molecular approach was adopted for the estimation of the intermolecular interaction energy, in its counterpoise-corrected version. Additionally, to gain insight into the nature of the Alq₃:polymer interaction, the SAPT0/def2-SVP interaction energy components were evaluated [35–37]. Frontier orbital energies and HOMO-LUMO gap values were estimated according to the recommendations of Scuseria *et al.* with the HSE06 screened density functional [38] for the geometries optimized within the ω B97X-D/def2-SVP approach. These calculations were carried out with the Gaussian16 program [39], while the SAPT0 decomposition was performed in PSI4 [40].

The vertical absorption spectra of the gas-phase systems were modelled by time-dependent DFT (TD-DFT) using the ω B97X-D functional in combination with the def2-SVP basis set. These TD-DFT calculations were performed in Q-Chem 5.2 [41] and the nature of the excited states was analysed based on the attachment and detachment densities [42]. These densities were computed using the libwfa module of Q-Chem [43]. The attachment and detachment densities were further analysed quantitatively using a python library for the analysis and visualization of electronic densities and transitions in molecules [44].

3. Results and discussion

3.1. Optical and structural characterisation

FTIR spectra of thin films of Alq₃ dispersed in PVK or PSS polymer matrix on a silicon substrate are shown in Fig. 3. FTIR measurements were performed to confirm the initial composition of Alq₃ in the selected polymer matrix. The characteristic vibration modes of the studied Alq₃:polymer layers are at: 450 cm⁻¹ (Al-N), 550–644 cm⁻¹ (Al-O) and band at about 740 cm⁻¹ (Al-O-Al) [45]. Three bands at 1109–1116 cm⁻¹, 1230 cm⁻¹, 1364–1380 cm⁻¹ are assigned to CH/CCN bending and CN tensile vibrations. The hydroxyquinol group is observed at 1460 and 1493 cm⁻¹, where these peaks correspond to CC/CN + CH bending stretch vibrations associated with both pyridyl and phenyl groups in Alq₃ [46]. In the higher wavenumber region, the IR transmittance peak centred at 1580–1595 cm⁻¹ is attributed to the CC stretching vibration involving the quinoline group of the ligands [47].

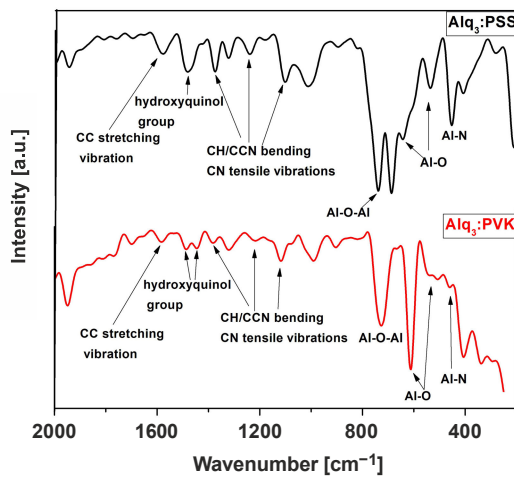


Fig. 3. FTIR transmittance spectrum of the Alq₃:polymer thin film.

The absorption and PL spectra of Alq₃:polymer (i.e., PSS or PVK) thin films are presented in Fig. 4. In the case of Alq₃:PVK, absorption is characterised by four bands with maximum at: 279 nm (B band), 382 nm (A band), 330 nm (C band), and 344 nm (D band). It should be noted that the A band is related to the transition from the ground state (S₀) to the first excited state (S₁) and is associated with charge transfer (CT) from the quinolate ring containing oxygen to the pyridyl ring. It is, therefore, attributed to the π - π^* excitation involving molecular orbitals of the quinolate ligands. The B band indicates the presence of the p-band related to the central metal atoms, where the p- π^* transition is more prominent [48]. The C and D bands are partly assigned to vibronic progression caused by the deformation mode of the electron transition ring. Additionally, these bands can be related to several other electronic transitions. For the Alq₃:PSS thin film, only three bands can be recognized: the B band visible at 278 nm, the C and D bands merge into a single band, and a very weak A band located at 381 nm [49]. From the theoretical calculations, three transitions are visible: from S₀ → S₁, S₀ → S₂, and S₀ → S₃ assigned to Alq₃. The first pass concerns the A band, while the second (and third) is assigned to the B band.

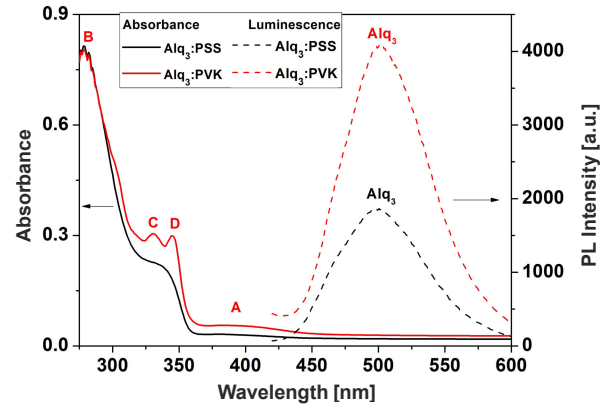


Fig. 4. Absorbance and PL spectra of the Alq₃:polymer. The absorption bands of Alq₃:PVK are labelled A – D, while the PL bands are labelled according to their assignment to different film components.

PL spectra of Alq₃:polymer thin films on a silicon substrate are shown in Fig. 4. After excitation, the thin layers emit a strong green light. The PL spectrum of Alq₃:PSS thin film shows the band at 500 nm, which corresponds to Alq₃. The emission bands for Alq₃:PVK at 502 nm refer to the recombination of excited states in Alq₃. The excited states responsible for PL in Alq₃ are localised in the ligands. The HOMO is localised on the phenoxide side and the LUMO on the pyridyl side [50]. As can be seen from Fig. 4, PL of Alq₃:PVK is much more intense than Alq₃:PSS.

The refractive index (n) and extinction index (k) of the Alq₃:PVK thin layer in the system: Alq₃:PVK/PEDOT:PSS/ITO/glass substrate were determined using SE. The experimentally obtained ellipsometric azimuths (Δ , Ψ) measured for three illumination angles (i.e., 60°, 65° and 70°) are plotted in Fig. 5 in individual colours. The theoretical characteristics using the Tauc-Lorentz model, corresponding to the best match to the experimental data, are drawn with black lines [34]. As can be seen, for each angle of illumination of the sample, a perfect match between theoretical and experimental characteristics was obtained.

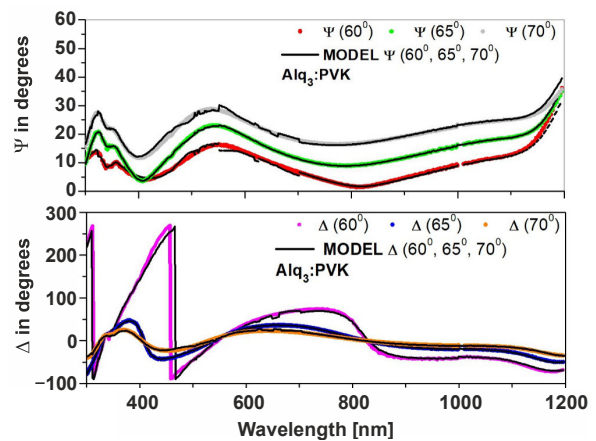


Fig. 5. Spectral dependence of Ψ and Δ azimuths for the Alq₃:PVK layer deposited on the PEDOT:PSS/ITO/glass.

The dispersion features of n and k obtained from the best fits are presented in Fig. 6. For wavelengths above 700 nm, the extinction coefficient is close to zero. As can be seen, in this spectral range, the refractive index shows normal dispersion. However, below 650 nm, k reaches very high values. In the course of its characteristics, the presence

of three absorption bands can be seen: the first one near 600 nm and other two located close to each other near the wavelength of 500 nm. The refractive index in this spectral range (i.e., $\lambda < 650$ nm) shows anomalous dispersion.

Figure 7 shows the SEM images of Alq₃ samples dispersed in PSS or PVK polymer matrix at a magnification of 500x. Both scans show surface smoothness and even distribution of Alq₃ grains on the surface of the sample, which is very important for OLED structures.

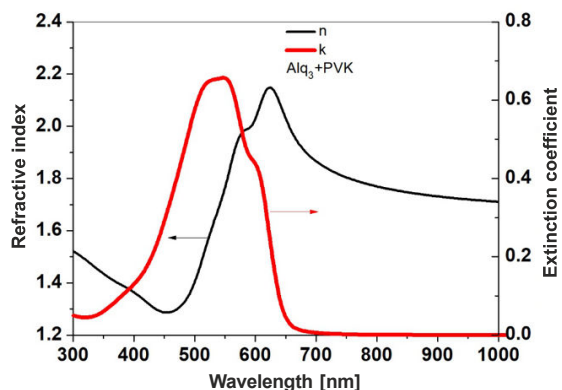


Fig. 6. Dependence of n and k for the Alq₃:PVK active layer on PEDOT:PSS/ITO/glass substrate.

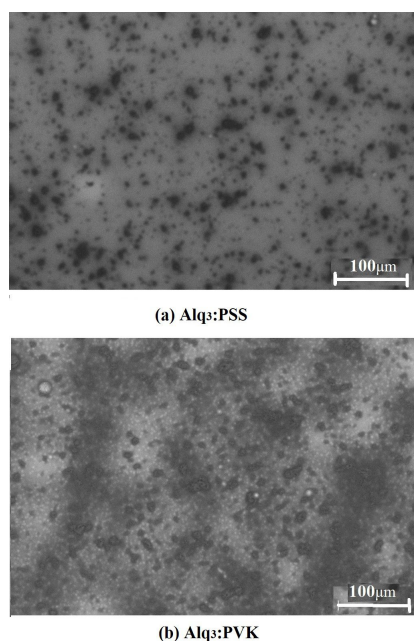


Fig. 7. The morphology of the investigated thin films.

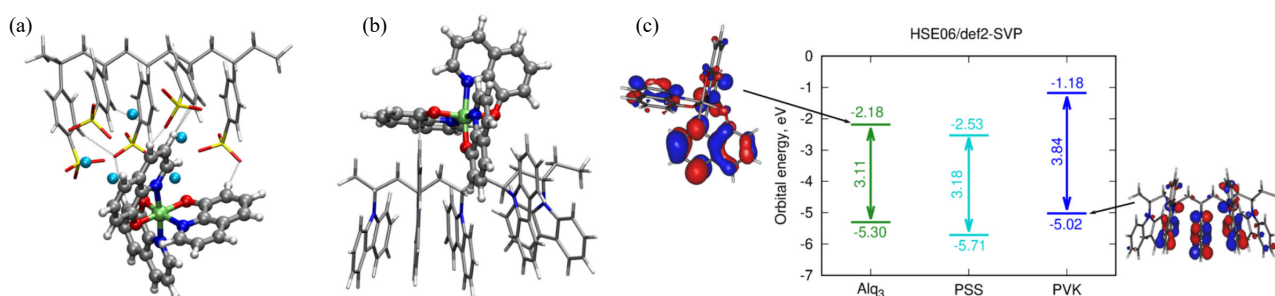


Fig. 8. The most stable mer-Alq₃:PSS (a) and mer-Alq₃:PVK (b) configurations used to model the Alq₃:polymer interface. The interaction energies obtained by SAPT0/def2-SVP approach are: (a) -78.37 kcal/mol, (b) -26.17 kcal/mol (CPK representation for Alq₃ molecule, cyan sodium ions, and licorice for the polymer chain). (c) Frontier orbital energy diagram for Alq₃ and polymer models from HSE06/def2-SVP calculations (energies for HOMO, LUMO and HOMO-LUMO gap in eV).

3.2. Quantum-chemical calculations

In order to determine which materials combination is more favourable for OLED applications, DFT calculations were performed to determine the possible structures of the Alq₃:polymer interface, as well as TD-DFT calculations to determine the nature of the lowest energy excited states. Several Alq₃:polymer configurations were considered, where the most stable among the exemplary optimized structures of Alq₃:polymer models are presented in Figs. 8(a) and 8(b) for PSS and PVK, respectively. The initial structures cover different directions of Alq₃ approaching the polymer chain. This strongly affects the interactions that govern the complex stabilization. For Alq₃ approaching the chain from the alkyl side, the weak interaction includes mostly the C–H...C and C–H...O contacts and the C–H... π interaction of the alkyl chain with the Alq₃ aromatic ring (compare Supplementary Information, Fig. S1). This arrangement leads to the weak super molecular interaction of -23.82 kcal/mol in the case of the mer-Alq₃:PSS complex [Fig. S1(a)] or -18.35 kcal/mol for fac-Alq₃:PSS [Fig. S1(d)]. Panels (b) and (e) of Fig. S1 present the Alq₃ reaching the polymer from the sulfonate groups and sodium ions, which intuitively increases the electrostatic interaction and creates an additional possibility of O...H–C contacts. The interaction energy estimated for this complex equals -32.40 kcal/mol for the fac isomer of Alq₃ and -81.15 kcal/mol for the mer-Alq₃:PSS complex. The strongest attraction between Alq₃ and PSS is observed when the aromatic quinolinato-ring enters deeper into the chain, featuring more stabilizing dispersion interactions. The total super molecular interaction energy for this case [Fig. S1(f) for fac-Alq₃:PSS] amounts to -75.69 kcal/mol. The strong interaction of Alq₃ with PSS is undoubtedly the result of the presence of the sodium ions, since PVK interaction with Alq₃ is significantly weaker than PSS with Alq₃, despite the similar size of the system.

In the case of PVK, Alq₃ approaching from the alkyl part of the chain [panel (a) and (d) of Fig. S2] gives the interaction energy of -30.90 kcal/mol for the mer-isomer and -26.55 kcal/mol for the fac-isomer. On the other side, Alq₃ interacting from the carbazole part of the chain [Fig. S2(c) and Fig. S2(e)] causes the insertion of the aromatic rings of Alq₃ between the carbazole moieties of polymer, thus maximizing the $\pi\pi$ stacking influence on the stability of the whole complex.

Table 1.

SAPT0/def2-SVP interaction energy components for the investigated systems [kcal/mol], the dispersion-to-electrostatic ratio and the character of the complex according to the Rezac criteria (ratio > 1.7: dispersion, ratio < 0.59: electrostatic, 0.59 < ratio < 1.7: mixed) [51].

Alq ₃ :PSS	Elst	Exch	Ind	Disp	Total	Disp/Elst	Character
mer-Alq ₃ :PSS(1)	-16.75	33.91	-6.92	-31.15	-20.91	1.9	Dispersion
mer-Alq ₃ :PSS(2)	-83.21	54.85	-24.72	-25.30	-78.37	0.3	Electrost.
mer-Alq ₃ :PSS(3)	-35.46	40.35	-10.85	-24.84	-30.81	0.7	Mixed
fac-Alq ₃ :PSS(1)	-13.73	26.47	-6.41	-23.02	-16.69	1.7	Dispersion
fac-Alq ₃ :PSS(2)	-34.66	50.32	-9.56	-26.88	-20.78	0.8	Mixed
fac-Alq ₃ :PSS(3)	-66.27	54.42	-24.06	-32.26	-68.18	0.5	Electrost.
mer-Alq ₃ :PVK(1)	-23.39	52.58	-8.33	-47.04	-26.17	2.0	Dispersion
mer-Alq ₃ :PVK(2)	-13.34	33.28	-4.40	-34.32	-18.78	2.6	Dispersion
mer-Alq ₃ :PVK(3)	-13.26	39.69	-4.41	-42.07	-20.05	3.2	Dispersion
fac-Alq ₃ :PVK(1)	-17.51	42.32	-5.93	-39.93	-21.06	2.3	Dispersion
fac-Alq ₃ :PVK(2)	-16.64	44.04	-5.68	-44.33	-21.61	2.8	Dispersion
fac-Alq ₃ :PVK(3)	-12.38	27.94	-6.11	-26.28	-16.83	2.1	Dispersion

Table 1 presents the decomposition of the total interaction energy into its components of different physical origin. It is clear that the direction from which Alq₃ is approaching the PSS chain strongly affects the electrostatic energy component. The influence on dispersion is weaker, and the three different models are governed by a different type of interaction. For the fac-Alq₃ isomers, the Alq₃:PSS (1) structure is governed by dispersion, Alq₃:PSS (2) features both, while Alq₃:PSS (3) is governed by electrostatic interactions, although its dispersion energy component is also the largest of the three. Similar tendency is observed in the case of mer-Alq₃ interactions with PSS: for complex (1), the dispersion component plays the most important role; in the case of complex (2), the electrostatic term is prevailing; and for complex (3), a balance between the electrostatic and dispersion components leads to a complex of mixed nature. On the other hand, the PVK complexes are governed mainly by the dispersion interaction, independently of the direction from which Alq₃ is approaching the polymer chain and the isomeric form of Alq₃. The electrostatic energy component is only weakly affected by a few kcal/mol.

The theoretical estimation of the parameters relevant for OLEDs involves the calculation of the frontier orbital energies of the donor and acceptor, namely polymer and Alq₃. The frontier molecular orbitals HOMO and LUMO of the donor and acceptor molecules play an important role in the functioning of OLED. The calculated values are given in Table S1 (see Supplementary Information) and presented in Fig. 8(c). The excellent agreement of the DFT results for Alq₃ in comparison to the experimental data extracted from electrochemical measurements can be noticed (see Table 2). Additionally, the functioning of OLED devices is also governed by the charge transfer between Alq₃ and polymer, which takes place at the interface. This charge transfer takes place in the excited state and is facilitated by delocalised orbitals, which extend over both electron donor and electron acceptor moieties. To compare Alq₃:PSS and Alq₃:PVK from this point of view, the absorption spectra of our model configurations were calculated and, for each, the nature of the ten lowest excited states was determined.

The average calculated vertical absorption spectra are shown in Fig. 9, where the spectra calculated for the two isomers and three considered configurations were averaged. In the case of Alq₃:PSS [Fig. 9(a)], the presence of the polymer does not significantly affect the absorption spectrum. There are small changes in the relative positions and intensities of the bands depending on the configuration, but these changes are quite minor.

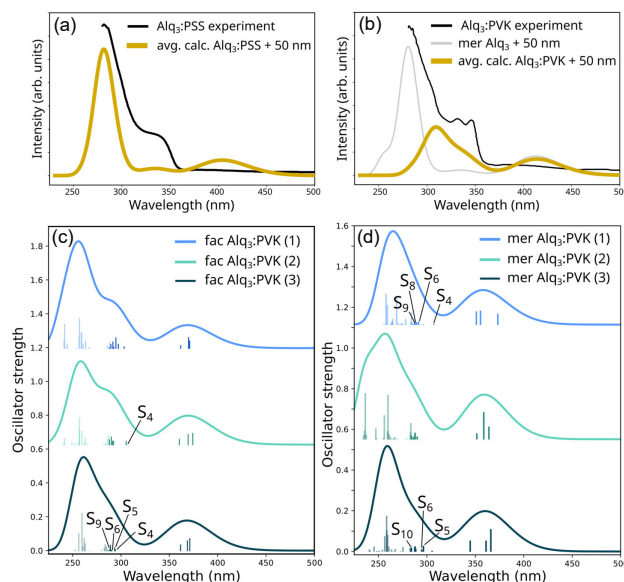


Fig. 9. Average vertical absorption spectrum for Alq₃:PSS (a) and Alq₃:PVK (b) calculated with the TD- ω B97X-D/def2-SVP approach in vacuum and shown in comparison to the experimentally measured absorption spectra of the film. The spectra have been obtained by taking the average of all the calculated configurations and shifted by 50 nm towards higher wavelengths to align the calculated main peak of Alq₃ with the experimental B band. It can be noted that, in the case of Alq₃:PVK, the lower wavelength region of the spectrum has not been captured, as not enough excitation vectors could be included in the calculations due to the large size of the system. Absorption spectra with bar graphs of fac-Alq₃:PVK (c) and mer-Alq₃:PVK (d), where the results have not been shifted. The lowest energy states with large CT between Alq₃ and polymer are marked.

The spectra of Alq₃:PVK are quite different compared to the single Alq₃ molecule, as new bands arise in the 325–375 nm region of the absorption spectrum [Fig. 9(b)]. To further analyse the origin of the peaks and nature of the excited states, a quantitative analysis of the attachment and detachment densities involved in the transitions were performed. The transition diagrams for all excited states are included in the [Supplementary Information](#). In the case of Alq₃:PSS, all of the analysed states are purely localised on the Alq₃ molecule and no CT excited states could be found. Instead, in the case of Alq₃:PVK, we could identify several excited states with large CT character between Alq₃ and PVK, marked in Figs. 9(c) and 9(d). Their corresponding transition diagrams are shown in Fig. 10. The diagrams for all analysed states can be found in the [Supplementary Information](#) (Fig. S4 and Fig. S5). In the case of fac-Alq₃:PVK model 1, i.e., when the Alq₃ molecule is located on the alkyl chain side of the polymer, most of the transitions were found to be localised either on Alq₃ or on PVK, and only one of the higher energy states had a minor CT character. A similar situation was obtained for mer-Alq₃:PVK model 2. For the other Alq₃:PVK models and isomer combinations, several states with large CT character were identified, as illustrated in Fig. 10. In essentially all of them, an electron located on the PVK polymer gets transferred to Alq₃. The absence of CT states in the case of Alq₃:PSS and the presence of these states in Alq₃:PVK indicates that Alq₃:PVK would provide a more favourable active material for OLED applications.

3.3. Optoelectronic characterisation

Figure 11 displays the cyclic voltammograms of the Alq₃ thin film. An oxidation potential onset of 1.22 V/ref was estimated. This value is associated to the ionization potential (IP) by the following equation $IP = E_{onset}^{ox} + 4.5$ [52], where E_{onset}^{ox} is the oxidation onset potential measured relative to the normal hydrogen electrode (NHE). According to Janak's theorem, the HOMO energy is typically considered to be equal to minus the value of the IP energy [53], hence, based on the oxidation potential onsets, we estimated the HOMO energies of Alq₃ thin films. The HOMO level of Alq₃ was at -5.925 eV.

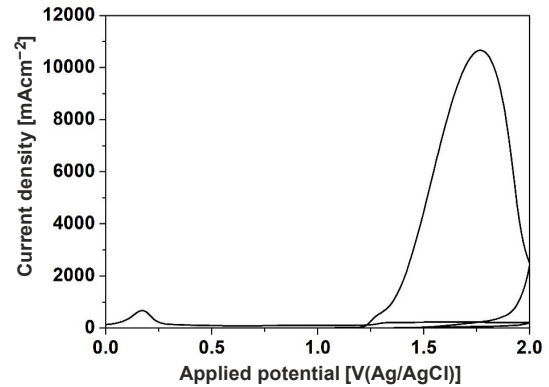


Fig. 11. Cyclic voltammetry of the Alq₃ thin film.

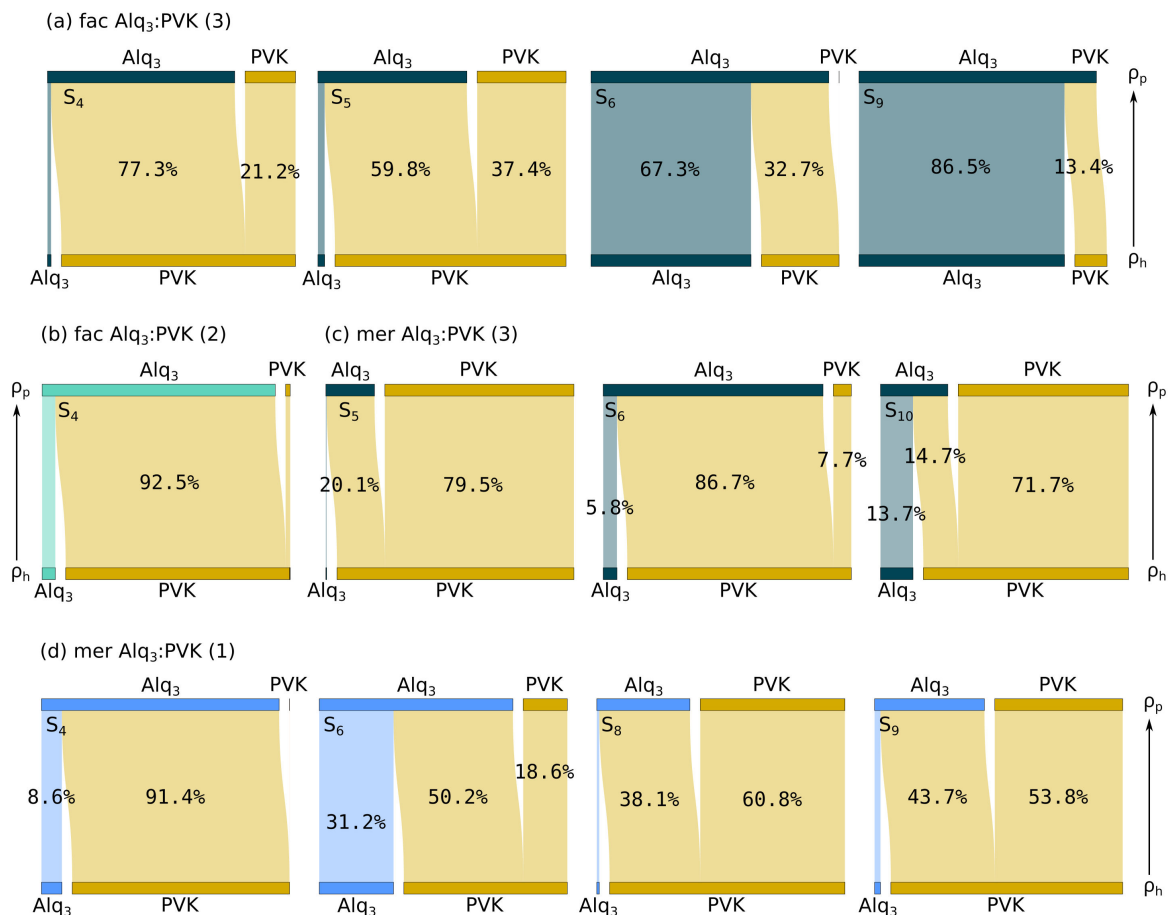


Fig. 10. Transition diagrams of the lowest energy excited states with large CT character for (a) fac-Alq₃:PVK model 3, fac-Alq₃:PVK model 2, (c) mer-Alq₃:PVK model 3, and (d) mer-Alq₃:PVK model 1.

According to the literature [54], Alq₃ has an optical band gap of 3.1 eV, thus, the LUMO level can be calculated by adding this value to the HOMO value. In this way, the LUMO level was located at -2.825 eV. All these values are presented in Table 2.

Table 2.
Electrochemical and energetic parameters of Alq₃ thin films.

	V _{onset,ox} [V/NHE]	IP [eV]	HOMO [eV]	E _{g,opt} [eV]	LUMO [eV]
Alq ₃	1.425	5.925	-5.925	3.1	-2.825

EL spectrum of the prepared simple OLED (i.e., glass/ITO/PEDOT:PSS/ Alq₃:PVK/Ca/Al, see Fig. 1) is shown in Fig. 12. It can be seen that OLED based on Alq₃:PVK exhibits a strong green EL emission that reaches the maximum at 520 nm (see Table 3).

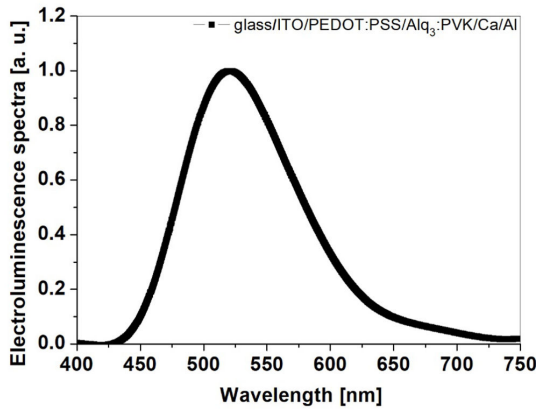


Fig. 12. EL spectrum of OLED, where Alq₃:PVK acts as an active layer in glass/ITO/PEDOT:PSS/Alq₃:PVK/Ca/Al.

Table 3 shows the maximum brightness values obtained for selected OLED structures with Alq₃. It was found that our structure (i.e., ITO/PEDOT:PSS/Alq₃:PVK/Ca/Al, where the thickness of Alq₃:PVK layer was about 103 nm) has a much better brightness value (1049 cd/m²) compared to other OLEDs. The maximum current efficiency (CE) of our OLED is equal to 0.86 cd/A. CE is the ratio of the brightness to the current of the OLED, i.e., the light efficiency taking into account the sensitivity of the human eye to various wavelengths of light in the visible range.

Table 3.
Selected parameters of manufactured OLED devices, where λ_{ELmax} – peak position of maximum EL emission, U_T – the threshold voltage, B_{max} – maximal brightness.

	λ_{ELmax} [nm]	U_T [V]	B_{max} [cd/m ²]	Ref.
PEDOT:PSS _(60nm) /Alq ₃ :PVK _(103nm) /Ca/Al	520	6.91	1049	this work
PVK _(100nm) /Alq ₃ _(26nm) /Al	525	16	75	[55]
PVK _(40nm) /Alq ₃ _(70nm) /Al	525	15	506	[55]
TPD _(50nm) /Alq ₃ _(40nm) /Al	–	12	250	[56]
TPD _(50nm) /Alq ₃ _(40nm) /LiF/Al	–	9	828	[56]

X. Jiang *et al.* [55] fabricated the ITO/PVK/Alq₃/Al structure, for which the obtained brightness values were respectively: 506 cd/m² and 75 cd/m² for the thickness of 110 nm (PVK = 40 nm, Alq₃ = 70 nm) and 130 nm (PVK = 110 nm, Alq₃ = 26 nm). They found that an increase in the thickness of the Alq₃ film and a decrease in the thickness of the PVK cause a significant increase in the brightness value. H. Mu *et al.* [56] present two OLED structures that differed by an additional LiF layer. They found that this addition layer increased the brightness value from 250 cd/m² (ITO/TPD/Alq₃/Al) to 828 cd/m² (ITO/TPD/Alq₃/LiF/Al).

Figures 13(a) and 13(b) show the luminance-voltage and the current density-voltage curves, respectively, measured for OLEDs prepared based on Alq₃:PVK. The luminance-voltage characteristics, presented in Fig. 13(a), show features typical of electroluminescent devices. Specifically, this is the characteristic rapid increase in luminance after exceeding a certain voltage threshold. Studied OLED exhibits a maximum brightness value of about 1049 cd/m² with a current efficiency of 0.86 cd/A. Figure 13(b) shows the current-voltage characteristics for the studied OLED. On the basis of this measurement, the threshold voltage U_T was determined (see Table 3) at 6.91 V.

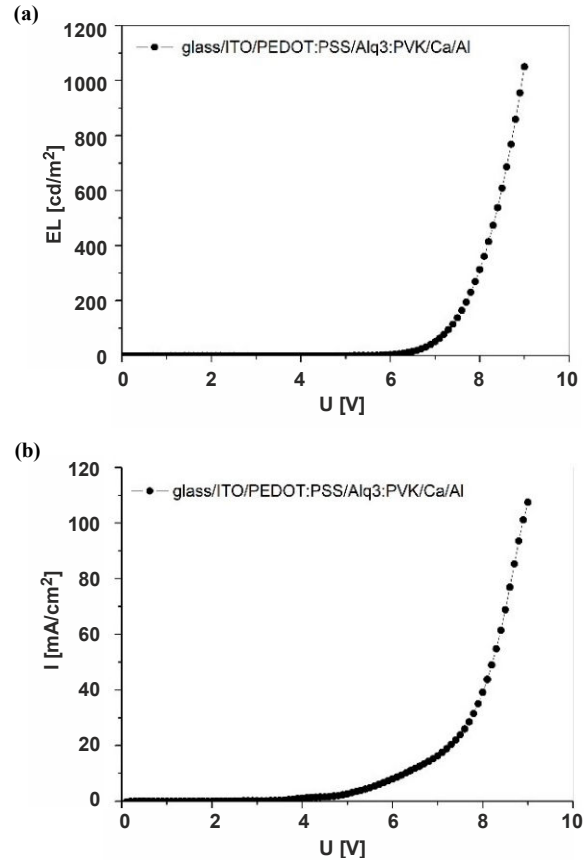


Fig. 13. Luminance-voltage characteristic for the studied OLED (a) and current density-voltage curve for the prepared OLED structure (b).

4. Conclusions

Thin layers of Alq₃ with PVK or PSS polymers were produced using the spin-coating method on glass and silicon substrates. FTIR measurements were performed to

confirm the composition. SEM images show that relatively smooth layers were obtained for the PVK and PSS polymers. The PL spectrum of the PSS polymer thin film has a band at 500 nm, which corresponds to Alq₃. The emission band for Alq₃:PVK at 502 nm relates to the recombination of excited states in Alq₃. OLEDs based on Alq₃:PVK exhibit strong EL emission with the green emission peak at 520 nm. Theoretically determined charge-transfer states present for Alq₃:PVK and their lack for Alq₃:PSS indicate the predicted better performance of Alq₃:PVK compared to Alq₃:PSS in OLEDs. OLED with the ITO/PEDOT:PSS/Alq₃:PVK/Ca/Al structure showed a maximum brightness value of about 1049 cd/m² with a CE of 0.86 cd/A. We found that the obtained maximum brightness value is much higher compared to other presented OLED structures.

Authors' statement

Research concept and design, R.S. and B.D.-Z.; collection and assembly of data, M.S., M.P.-K., A.K.-K., I.E.B., V.F., E.G. A.A., and B.D.-Z.; data analysis and interpretation, M.S., M.P.-K., A.K.-K., I.E.B., V.F., E.G., R.S., A.A., and B.D.-Z.; writing the article, M.S., A.K.-K., and I.E.B.; critical revision of the article, R.S., I.E.B., and B.D.-Z.; final approval of article, A.K.-K., I.E.B., E.G. A.A., P.S., J.L., R.S., and B.D.-Z.

Acknowledgements

M.S., A.A., and B.D.-Z. thank the NAWA PHC Polonium Project (no. BPN/BFR/2021/1/00036). Wrocław Center for Networking and Supercomputing (WCSS) is gratefully acknowledged for the generous allotment of computational resources. The TD-DFT calculations were made possible by resources provided by the Swedish National Infrastructure for Computing (SNIC) at NSC, partially funded by the Swedish Research Council through grant agreement no. 2018–05973. We also made use of the local cluster of the Chemistry Department at NCU (Argon) and I.E.B. is very grateful to Dariusz Kędziera for access and help with running calculations on this cluster.

References

- [1] Cho, C. P., Wu, C. A. & Perng, T. P. Crystallization of amorphous tris (8-hydroxyquinoline) aluminum nanoparticles and transformation to nanowires. *Adv. Funct. Mater.* **16**, 819–823 (2006). <https://doi.org/10.1002/adfm.200500631>
- [2] Xie, G. *et al.* Highly efficient top-emitting white organic light-emitting diodes with improved contrast and reduced angular dependence for active matrix displays. *Org. Electron.* **11**, 2055–2059 (2010). <https://doi.org/10.1016/j.orgel.2010.10.001>
- [3] Du, J. *et al.* Instability origin and improvement scheme of facial Alq₃ for blue OLED application. *Chem. Res. Chin. Univ.* **32**, 423–427 (2016). <https://doi.org/10.1007/s40242-016-5485-z>
- [4] Mitschke, U. & Bäuerle, P. The electroluminescence of organic materials. *J. Mater. Chem.* **10**, 1471–1507 (2000). <https://doi.org/10.1039/A908713C>
- [5] Feast, W. J., Tsibouklis, J., Pouwer, K. L., Groenendaal, L. & Meijer, E. W. Synthesis, processing and material properties of conjugated polymers. *Polymer* **37**, 5017–5047 (1996). [https://doi.org/10.1016/0032-3861\(96\)00439-9](https://doi.org/10.1016/0032-3861(96)00439-9)
- [6] Burroughes, J. H. *et al.* Light-emitting diodes based on conjugated polymers. *Nature* **347**, 539–541 (1990). <https://doi.org/10.1038/347539a0>

- [7] Kirchmeyer, S. & Reuter, K. J. Scientific importance, properties and growing applications of poly(3,4-ethylenedioxythiophene). *J. Mater. Chem.* **15**, 2077–2088 (2005). <https://doi.org/10.1039/B417803N>
- [8] Kim, Y. H. *et al.* Highly conductive PEDOT:PSS electrode with optimized solvent and thermal post-treatment for ITO-free organic solar cells. *Adv. Funct. Mater.* **21**, 1076–1081 (2011). <https://doi.org/10.1002/adfm.201002290>
- [9] Takano, T., Masunaga, H., Fujiwara, A., Okuzaki, H. & Sasaki, T. PEDOT nanocrystal in highly conductive PEDOT:PSS polymer films. *Macromolecules* **45**, 3859–865 (2012). <https://doi.org/10.1021/ma300120g>
- [10] Tian, Y. *et al.* High-performance transparent PEDOT: PSS/CNT films for OLEDs. *Nanomaterials* **11**, 1–17 (2021). <https://doi.org/10.3390/nano11082067>
- [11] Jeltsch, K., Lupa, G. & Weitz, R. T. Materials depth distribution and degradation of a Flrpic based solution-processed blue OLED. *Org. Electron.* **26**, 365–370 (2015). <https://doi.org/10.1016/j.orgel.2015.08.003>
- [12] Yu, S. Y., Chang, J. H., Wang, P. S., Wu, C. I. & Tao, Y. T. effect of ITO surface modification on the oled device lifetime. *Langmuir* **30**, 7369–7376 (2014). <https://doi.org/10.1021/la4049659>
- [13] Shen, Z., Burrows, P. E., Bulović, V., Forrest, S. R. & Thompson, M. E. Three-color, tunable, organic light-emitting devices. *Science* **276**, 2009–2011 (1997). <https://doi.org/10.1126/science.276.5321.2009>
- [14] Bi, H. *et al.* Fac-Alq₃ and Mer-Alq₃ nano/ microcrystals with different emission and charge transporting properties. *Adv. Mater.* **22**, 1631–1634 (2010). <https://doi.org/10.1002/adma.200903094>
- [15] Halls, M. D. & Schlegel, H. B. Molecular orbital study of the first excited state of the OLED material Tris(8-hydroxyquinoline)aluminum(III). *Chem. Mater.* **13**, 2632–2640 (2001). <https://doi.org/10.1021/cm010121d>
- [16] Kato, T., Mori, T. & Mizutani, T. Effect of fabrication conditions on photoluminescence and absorption of hole transport materials. *Thin Solid Films* **393**, 109–113 (2001). [https://doi.org/10.1016/S0040-6090\(01\)01112-9](https://doi.org/10.1016/S0040-6090(01)01112-9)
- [17] Lee, Y. H. *et al.* effect of deposition rate of organic layer on electrical and optical characteristics of OLEDs. *Mol. Cryst. Liq. Cryst.* **462**, 143–148 (2007). <https://doi.org/10.1080/07370650601013088>
- [18] Zhang, D. *et al.* Highly efficient hybrid warm white organic light-emitting diodes using a blue thermally activated delayed fluorescence emitter: exploiting the external heavy-atom effect. *Light: Sci. Appl.* **4**, e232-1-e232-7 (2015). <https://doi.org/10.1038/lsa.2015.5>
- [19] Aziz, H., Popovic, Z. D., Hu, N. X., Hor, A. M. & Xu, G. Degradation mechanism of small molecule-based organic light-emitting devices. *Science* **283**, 1900–1902 (1999). <https://doi.org/10.1126/science.283.5409.1900>
- [20] Prez-Bolvar, C., Takizawa, S., Nishimura, G., Montes, V. A. & Anzenbacher, P. High-efficiency Tris(8-hydroxyquinoline) aluminum (Alq₃) complexes for organic white-light-emitting diodes and solid-state lighting. *Chem. Eur. J.* **17**, 9076–9082 (2011). <https://doi.org/10.1002/chem.201100707>
- [21] Zhang, Y., Hu, Y., Chen, J., Zhou, Q. & Ma, D. Charge carrier injection and transport in PVK:Alq₃ blend films. *J. Phys. D* **36**, 2006–2009 (2003). <https://doi.org/10.1088/0022-3727/36/16/313>
- [22] Fukushima, T. & Kaji, H. Green- and blue-emitting tris(8-hydroxyquinoline) aluminum(III) (Alq₃) crystalline polymorphs: Preparation and application to organic light-emitting diodes. *Org. Electron.* **13**, 2985–2990 (2012). <https://doi.org/10.1016/j.orgel.2012.08.036>
- [23] Dalasiński, P., Lukasiak, Z., Wojdyła, M., Rębarz, M. & Bała, W. Study of optical properties of TRIS (8-hydroxyquinoline) aluminum (III). *Opt. Mat.* **28**, 98–101 (2006). <https://doi.org/10.1016/j.optmat.2004.10.031>
- [24] Duan, L., Yang, H., Wang, G. & Duan, Y. Preparation of 8-hydroxyquinoline aluminum nanomaterials to enhance properties for green organic light-emitting diode devices. *J. Soc. Inf. Display* **29**, 466–475 (2021). <https://doi.org/10.1002/jsid.986>
- [25] Karbovnyk, I. *et al.* Optical properties of composite structure based on ZnO microneedles and Alq₃ thin film. *Opt. Quantum Electron.* **53**, 1–9 (2021). <https://doi.org/10.1007/s11082-021-03292-1>
- [26] Pope, M. & Swenberg, C. E. *Electronic Processes In Organic Crystals And Polymers 2nd ed.* (Oxford University Press, New York 1993).
- [27] D'Almeida, K. *et al.* Carbazole-based electroluminescent devices obtained by vacuum evaporation. *J. Appl. Polym. Sci.* **82**, 2042–2055 (2001). <https://doi.org/10.1002/app.2050>

- [28] D'Angelo, P. *et al.* Electrical transport properties characterization of PVK (poly N-vinylcarbazole) for electroluminescent devices applications. *Solid-State Electron.* **51**, 123–129 (2007). <https://doi.org/10.1016/j.sse.2006.11.008>
- [29] Bießmann, L. *et al.* Monitoring the swelling behavior of PEDOT: PSS electrodes under high humidity conditions. *ACS Appl. Mater. Interfaces* **10**, 9865–9872 (2018). <https://doi.org/10.1021/acsami.8b00446>
- [30] Bießmann, L. *et al.* Highly conducting, transparent PEDOT:PSS polymer electrodes from post-treatment with weak and strong acids. *Adv. Electron. Mater.* **5**, 1800654-1-1800654-10 (2019). <https://doi.org/10.1002/aelm.201800654>
- [31] Fehse, K. *et al.* Lifetime of organic light emitting diodes on polymer anodes. *Appl. Phys. Lett.* **93**, 83303-1-83303-3 (2008). <https://doi.org/10.1063/1.2975369>
- [32] Derkowska-Zielinska, B. *et al.* Photovoltaic cells with various azo dyes as components of the active layer. *Sol. Energy* **203**, 19–24 (2020). <https://doi.org/10.1016/j.solener.2020.04.022>
- [33] Gašiorski, P. *et al.* Efficient green electroluminescence from 1,3-diphenyl-1H-pyrazolo[3,4-b] quinoxaline dyes in dye-doped polymer based electroluminescent devices. *Dyes Pigm.* **151**, 380–384 (2018). <https://doi.org/10.1016/j.dyepig.2018.01.002>
- [34] Abdel-Wahab, F., Merazga, A., Rasheedy, M. S. & Montaser, A. A. Optical characterization of the annealing effect on Ge₅Te₂₀Se₇₅ thin films by variable angle of incidence spectroscopic ellipsometry. *Optik* **127**, 3871–3877 (2016). <https://doi.org/10.1016/j.ijleo.2016.01.064>
- [35] Jeziorski, B., Moszynski, R. & Szalewicz, K. Perturbation theory approach to intermolecular potential energy surfaces of van der Waals complexes. *Chem. Rev.* **94**, 1887–1930 (1994). <https://doi.org/10.1021/cr00031a008>
- [36] Hohenstein, E. G., Parrish, R. M., Sherrill, C. D., Turney, J. M. & Schaefer, H. F. Large-scale symmetry-adapted perturbation theory computations via density fitting and laplace transformation techniques: investigating the fundamental forces of DNA-intercalator interactions. *J. Chem. Phys.* **135**, 174017 (2011). <https://doi.org/10.1063/1.3656681>
- [37] Hohenstein, E. G. & Sherrill, C. D. Density fitting and cholesky decomposition approximations in symmetry-adapted perturbation theory: implementation and application to probe the nature of π - π interactions in linear acenes. *J. Chem. Phys.* **132**, 184111 (2010). <https://doi.org/10.1063/1.3426316>
- [38] Garza, A. J. & Scuseria, G. E. Predicting band gaps with hybrid density functionals. *J. Phys. Chem. Lett.* **7**, 4165–4170 (2016). <https://doi.org/10.1021/acs.jpcclett.6b01807>
- [39] Frisch, M. J. *et al.* *Gaussian 16, Revision B.01.* (Gaussian, Inc., Wallingford, CT, 2016).
- [40] Turney, J. M. *et al.* Psi4: An open-source *ab initio* electronic structure program. *WIREs Comput. Mol. Sci.* **2**, 556 (2012). <https://doi.org/10.1002/wcms.93>
- [41] Epifanovsky, E. *et al.* Software for the frontiers of quantum chemistry: An overview of developments in the Q-Chem 5 package. *J. Chem. Phys.* **155**, 084801 (2021). <https://doi.org/10.1063/5.0055522>
- [42] Head-Gordon, M., Grana, A. M., Maurice, D. & White, C. A. Analysis of electronic transitions as the difference of electron attachment and detachment densities. *J. Chem. Phys.* **99**, 14261–14270 (1995). <https://doi.org/10.1021/j100039a012>
- [43] Plasser, F., Dreuw, A. & Krylov, A. libwfa: Wavefunction analysis tools for excited and open-shell electronic states. *WIREs Comput. Mol. Sci.* **12**, e1595 (2022). <https://doi.org/10.1002/wcms.1595>
- [44] Masood, T. B. *et al.* Visual analysis of electronic densities and transitions in molecules, computer graphics forum. *Anal. Sci. Eng.* **40**, 287–298 (2021). <https://doi.org/10.1111/cgf.14307>
- [45] Cuba, M. & Muralidharan, G. Enhanced luminescence properties of hybrid Alq₃/ZnO (organic/inorganic) composite films. *J. Lumin.* **156**, 1–7 (2014). <https://doi.org/10.1016/j.jlumin.2014.07.008>
- [46] Muhammad, F. F., Hapip, A. I. A. & Sulaiman, K. Study of optoelectronic energy bands and molecular energy levels of tris-(8-hydroxyquinolate) gallium and aluminum organometallic materials from their spectroscopic and electrochemical analysis. *J. Organom. Chem.* **695**, 2526–2531 (2010). <https://doi.org/10.1016/j.jorganchem.2010.07.026>
- [47] Koay, J. Y., Sharif, K. A. M. & Rahman, S. A. Influence of film thickness on the structural, electrical and photoluminescence properties of vacuum deposited Alq₃ thin films on c-silicon substrate. *Thin Solid Films* **517**, 5298–5300 (2009). <https://doi.org/10.1016/j.tsf.2009.03.145>
- [48] Derkowska-Zielinska, B. Enhancement of third order nonlinear optical susceptibility of Alq₃ in polar aprotic solvents. *Opt. Lett.* **42**, 567–570 (2017). <https://doi.org/10.1364/OL.42.000567>
- [49] Sypniewska, M. *et al.* Optical and morphological properties of ZnO and Alq₃ incorporated polymeric thin layers fabricated by the dip-coating method. *Appl. Nanosci.* 1–10 (2022). <https://doi.org/10.1007/s13204-022-02647-8>
- [50] Ravi Kishore, V. V. N. *et al.* On the assignment of the absorption bands in the optical spectrum of Alq₃. *Synth. Met.* **126**, 199–205 (2002). [https://doi.org/10.1016/S0379-6779\(01\)00553-7](https://doi.org/10.1016/S0379-6779(01)00553-7)
- [51] Řezáč, J., Riley, K. E. & Hobza, P. S66: A well-balanced database of benchmark interaction energies relevant to biomolecular structures. *J. Chem. Theory Comput.* **7**, 2427–2438 (2011). <https://doi.org/10.1021/ct2002946>
- [52] Cermi, R. *et al.* Electrochemical and optical studies of PPV derivatives and poly(aromatic oxadiazoles). *Synth. Met.* **84**, 359–360 (1997). [https://doi.org/10.1016/S0379-6779\(97\)80781-3](https://doi.org/10.1016/S0379-6779(97)80781-3)
- [53] Amati, M., Stoia, S. & Baerends, E. J. The electron affinity as the highest occupied anion orbital energy with a sufficiently accurate approximation of the exact Kohn-Sham potential. *J. Chem. Theory Comput.* **16**, 443–452 (2020). <https://doi.org/10.1021/acs.jctc.9b00981>
- [54] Freitas, A. R. *et al.* Synthesis, structure, spectral and electrochemical properties of chromium(III) tris-(8-hydroxyquinolate). *Dalton Trans.* **44**, 11491–11503 (2015). <https://doi.org/10.1039/C5DT00727E>
- [55] Jiang, X., Liu, Y., Song, X. & Zhu, D. Organic light-emitting diodes made with poly(N-vinylcarbazole) and 8-hydroxyquinoline aluminium (Alq₃). *Synth. Met.* **87**, 175–178 (1997). [https://doi.org/10.1016/S0379-6779\(97\)80104-X](https://doi.org/10.1016/S0379-6779(97)80104-X)
- [56] Mu, H., Li, W., Jones, R., Steckl, A. & Klotzkin, D. A comparative study of electrode effects on the electrical and luminescent characteristics of Alq₃/TPD OLED: Improvements due to conductive polymer (PEDOT) anode. *J. Lumin.* **126**, 225–229 (2007). <https://doi.org/10.1016/j.jlumin.2006.07.00>

Supplementary Information

Table S1.

Energies of frontier orbitals HOMO and LUMO and HOMO-LUMO gap [eV] and open-circuit voltage, U_{OC}, estimated with the HSE06 functional for polymers and Alq₃ (the experimental Alq₃ band gap equal to 3.1 eV [54] serves as a reference point for the quality of the DFT calculations).

	def2-SVP			def2-TZVP		
	Alq ₃	PSS	PVK	Alq ₃	PSS	PVK
HOMO	-5.30	-5.71	-5.02	-5.33		
LUMO	-2.19	-2.53	-1.18	-2.24		
Gap	3.11	3.18	3.84	3.10		
U _{OC}		-3.52	-2.83			

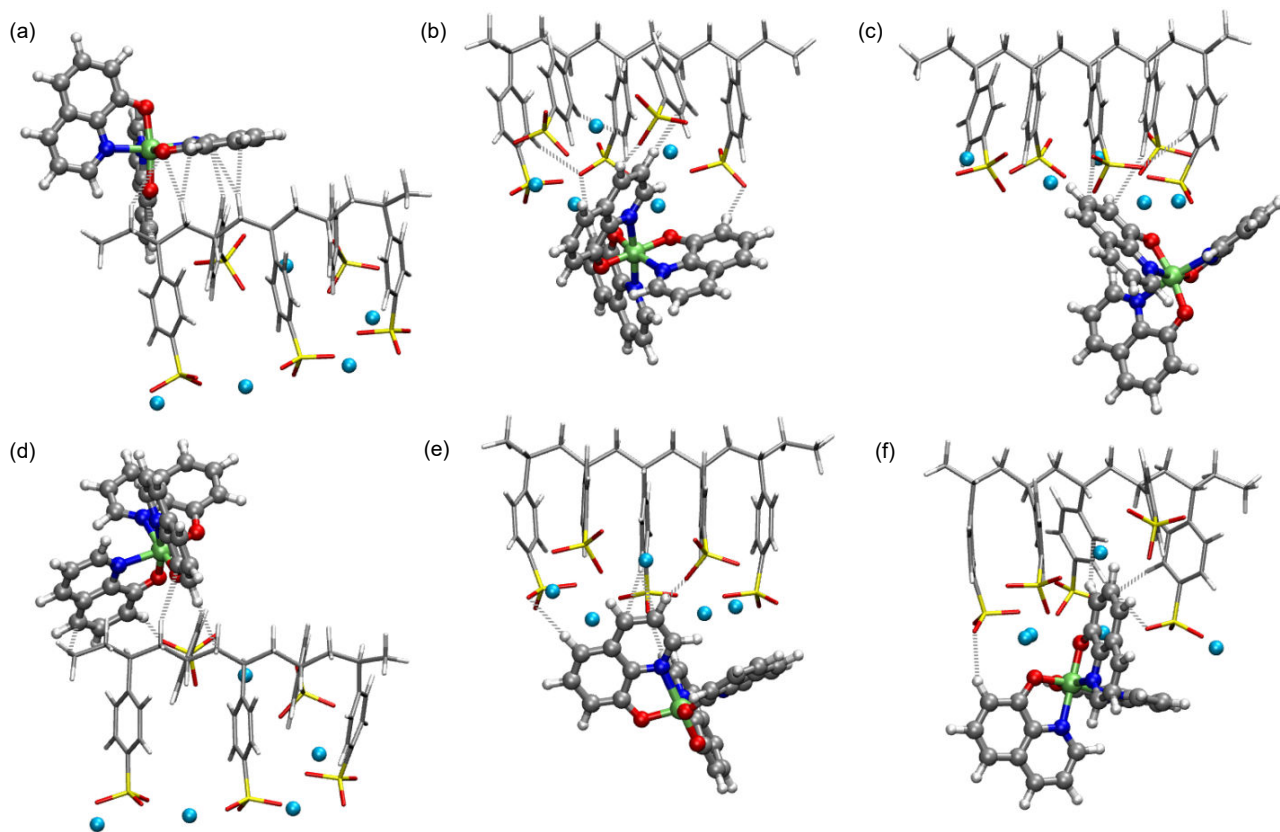


Fig. S1. Optimized exemplary structures of PSS complexes with mer-Alq₃ (a)–(c) and fac-Alq₃ (d)–(f) calculated using ω B97X-D/def2-SVP; Na⁺ cations and Alq₃ and presented in the CPK mode and polymer chain fragment as licorice.

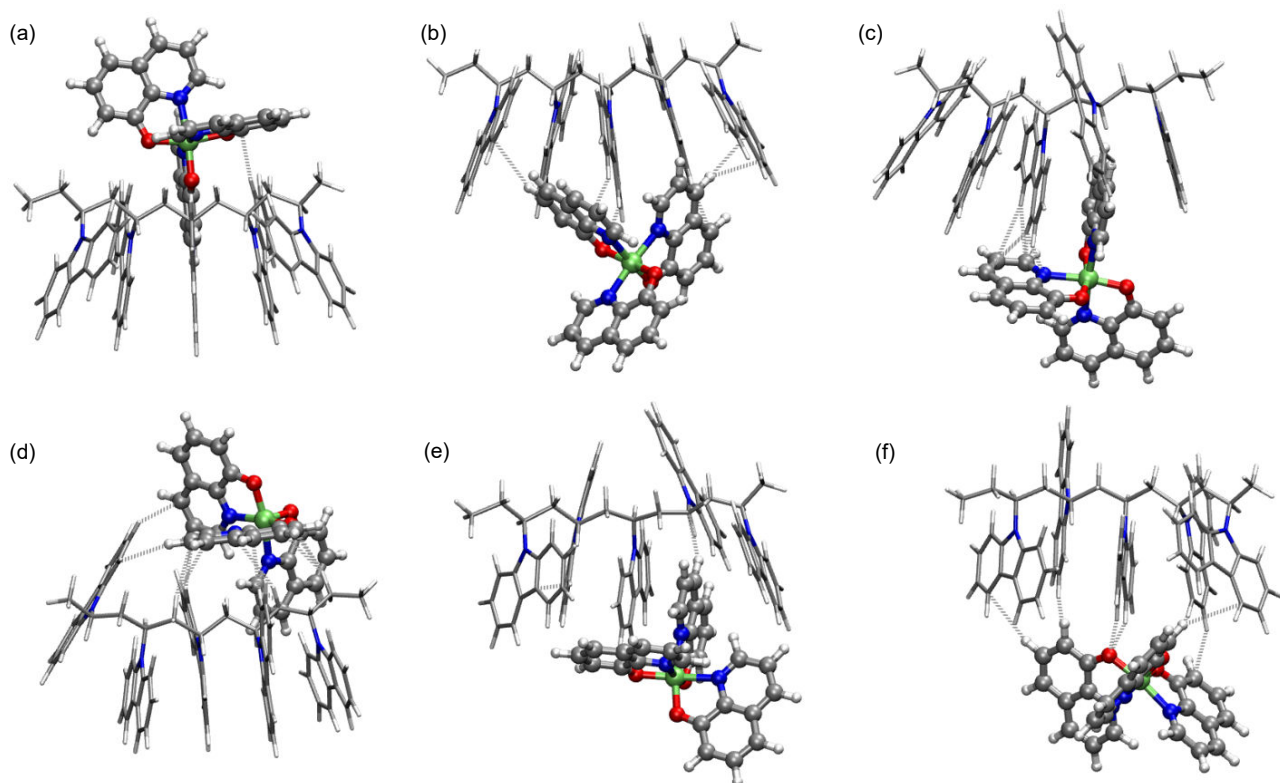


Fig. S2. Optimized exemplary structures of PVK complexes with mer-Alq₃ (a)–(c) and fac-Alq₃ (d)–(f) calculated using ω B97X-D/def2-SVP; Alq₃ is shown in the CPK mode and polymer chain fragment as licorice.

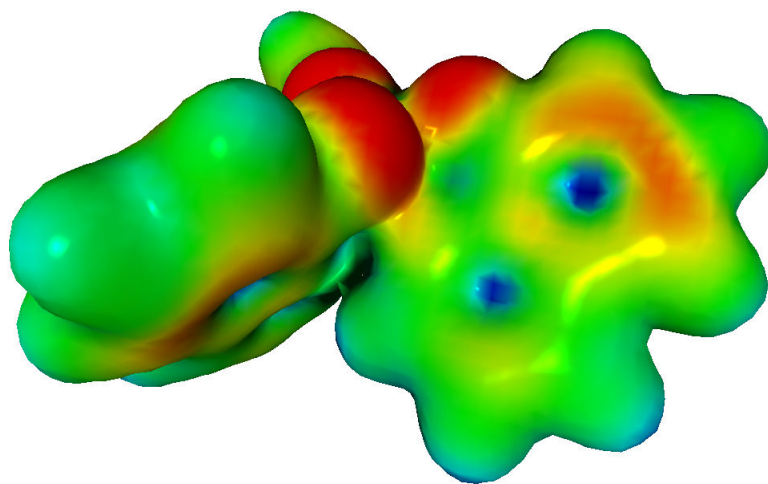


Fig. S3. Multipole derived electrostatic potential of Alq₃ estimated by the ω B97X-D/def2-SVP approach

NEXT PAGE

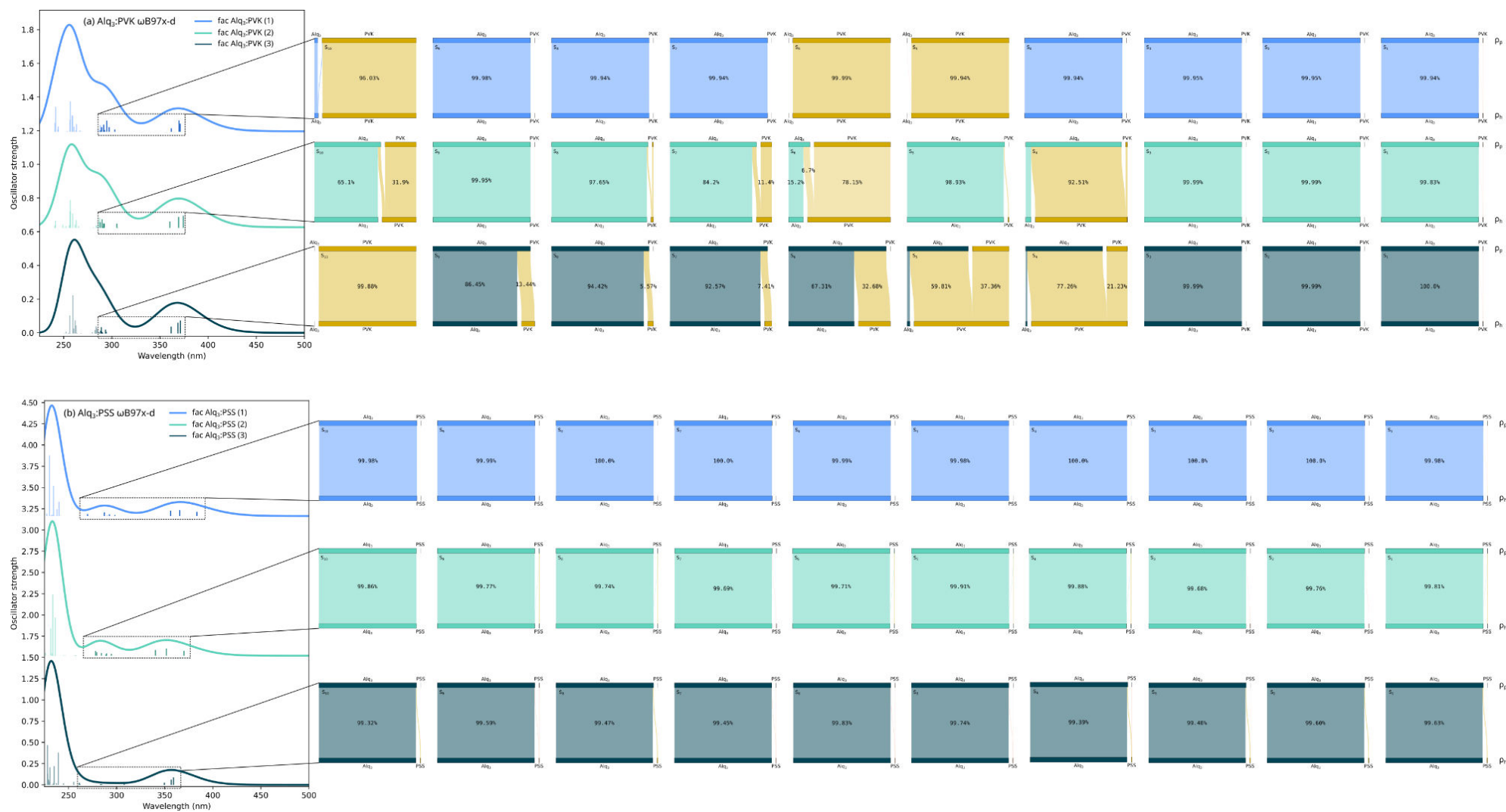


Fig. S4. Transition diagrams for all analysed states of fac-Alq₃:polymer.

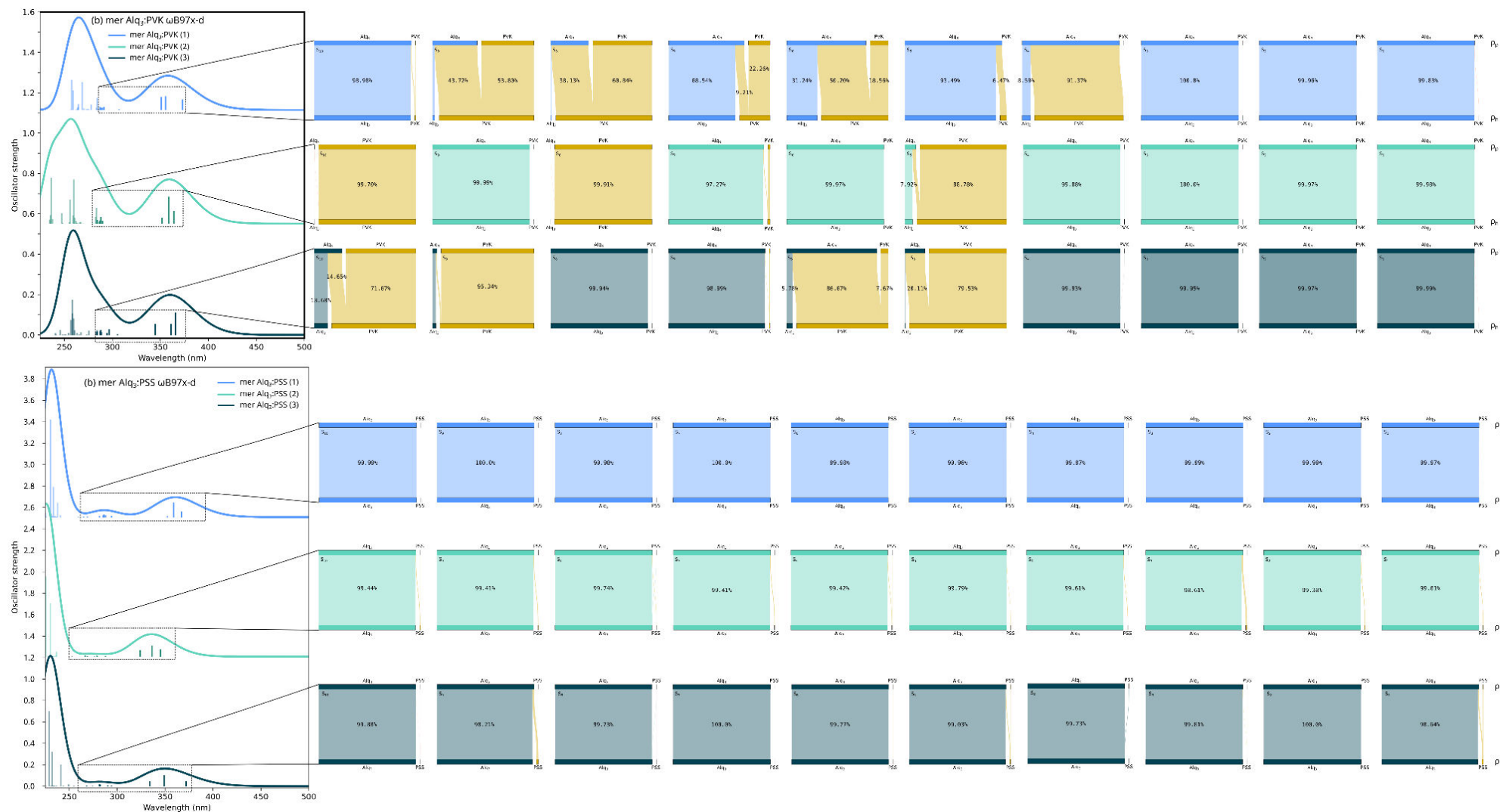


Fig. S5. Transition diagrams for all analysed states of mer-Alq₃:polymer.